Supplement of Earth Surf. Dynam., 9, 923–935, 2021
https://doi.org/10.5194/esurf-9-923-2021-supplement
© Author(s) 2021. CC BY 4.0 License.

Supplement of

Last-glacial-cycle glacier erosion potential in the Alps

Julien Seguinot and Ian Delaney

Correspondence to: Julien Seguinot (julien-alps-erosion@posteo.eu)

The copyright of individual parts of the supplement might differ from the article licence.

Supplementary figures

This document contains copies of the main text Figs. 1–5, and their equivalent using the other tested erosion laws. Note that colour levels and vertical axes were adapted to the magnitude of the results. Potential erosion rates aggregated in time, space and elevation bands, and used to plot these figures were made available in a long-term online archive (Seguinot, 2021, https://doi.org/10.5281/zenodo.4495419).

List of Figures

S1 Cumulative erosion potential and annual erosion volume after Koppes et al. (2015), same as main text Fig. 1. . 2
S2 Cumulative erosion potential and annual erosion volume after Herman et al. (2015). 3
S3 Cumulative erosion potential and annual erosion volume after Humphrey and Raymond (1994) 4
S4 Cumulative erosion potential and annual erosion volume after Cook et al. (2020) 5
S5 Potential erosion volume in relation to ice volume after Koppes et al. (2015), same as main text Fig. 2. 6
S6 Potential erosion volume in relation to ice volume after Herman et al. (2015). 6
S7 Potential erosion volume in relation to ice volume after Humphrey and Raymond (1994). 6
S8 Potential erosion volume in relation to ice volume after Cook et al. (2020). 6
S9 Rhine Glacier potential erosion rate over time after Koppes et al. (2015), same as main text Fig. 3. 7
S10 Rhine Glacier potential erosion rate over time after Herman et al. (2015). 7
S11 Rhine Glacier potential erosion rate over time after Humphrey and Raymond (1994). 8
S12 Rhine Glacier potential erosion rate over time after Cook et al. (2020). 8
S13 Potential erosion rate per altitude band after Koppes et al. (2015), same as main text Fig. 4. 9
S14 Potential erosion rate per altitude band after Herman et al. (2015). 9
S15 Potential erosion rate per altitude band after Humphrey and Raymond (1994). 10
S16 Potential erosion rate per altitude band after Cook et al. (2020). 10
S17 Climate sensitivity of cumulative erosion potential after Koppes et al. (2015), same as main text Fig. 5. 11
S18 Climate sensitivity of cumulative erosion potential after Herman et al. (2015). 11
S19 Climate sensitivity of cumulative erosion potential after Humphrey and Raymond (1994) 12
S20 Climate sensitivity of cumulative erosion potential after Cook et al. (2020) 12

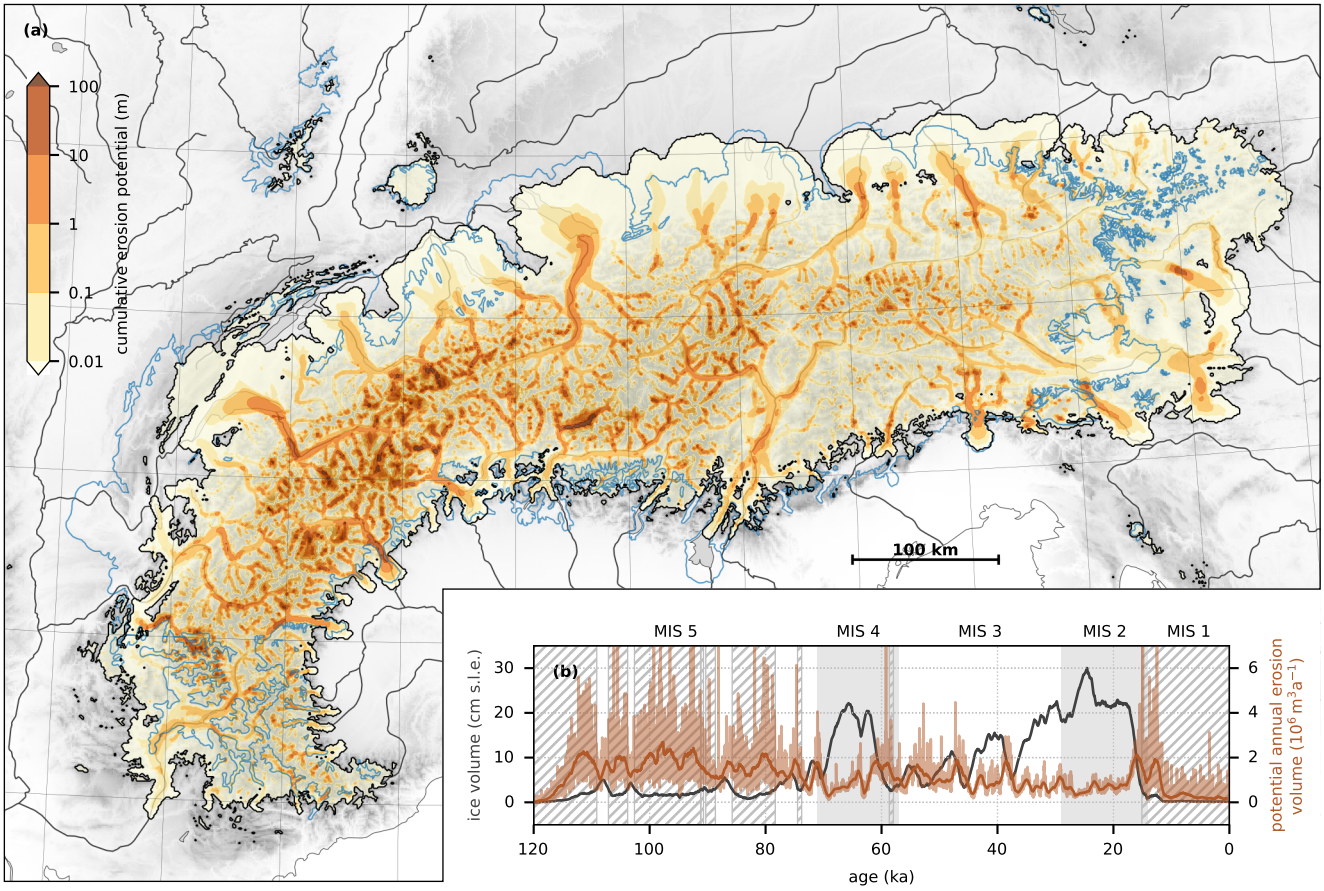

Figure S1. **(a)** Modelled cumulative (time-integrated) glacial erosion potential over the last glacial cycle and geomorphological reconstruction of Last Glacial Maximum Alpine glacier extent for comparison (solid blue line, Ehlers et al., 2011). The background maps consists of the initial basal topography from SRTM (Jarvis et al., 2008) and Natural Earth Data (Patterson and Kelso, 2017). **(b)** Modelled total ice volume in centimetres of sea-level equivalent (cm s.l.e., black), annual (domain-integrated) potential erosion volume (light brown) and its 1-ka running mean (dark brown). Shaded gray areas indicate the timing for MIS 2 and 4 (Lisiecki and Raymo, 2005). Hatches mark periods with ice volume below 3 cm s.l.e. where glacier sliding may be affected by stress-balance approximations and model horizontal resolution. After Koppes et al. (2015), same as main text Fig. 1.

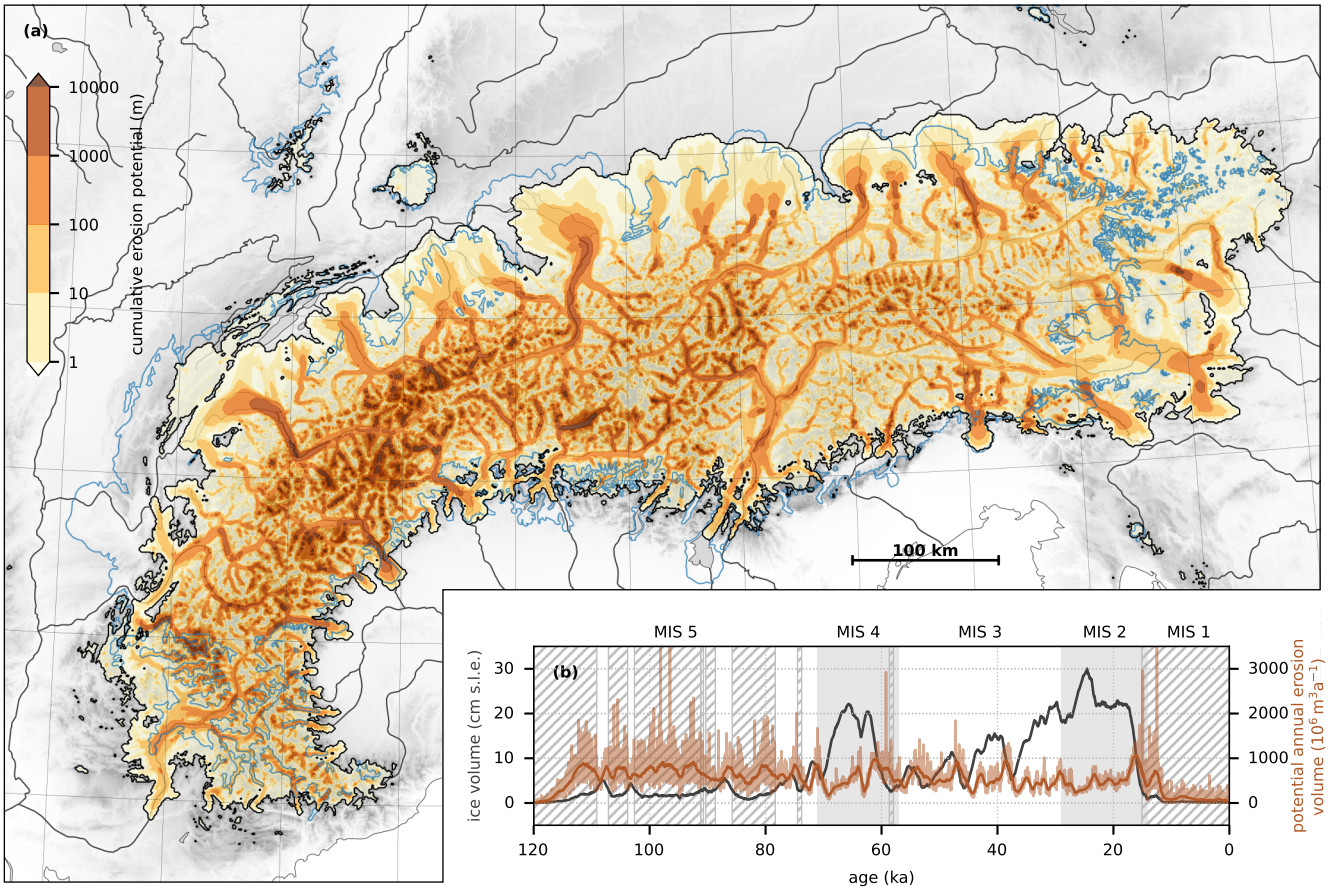

Figure S2. Cumulative erosion potential and annual erosion volume after Herman et al. (2015).

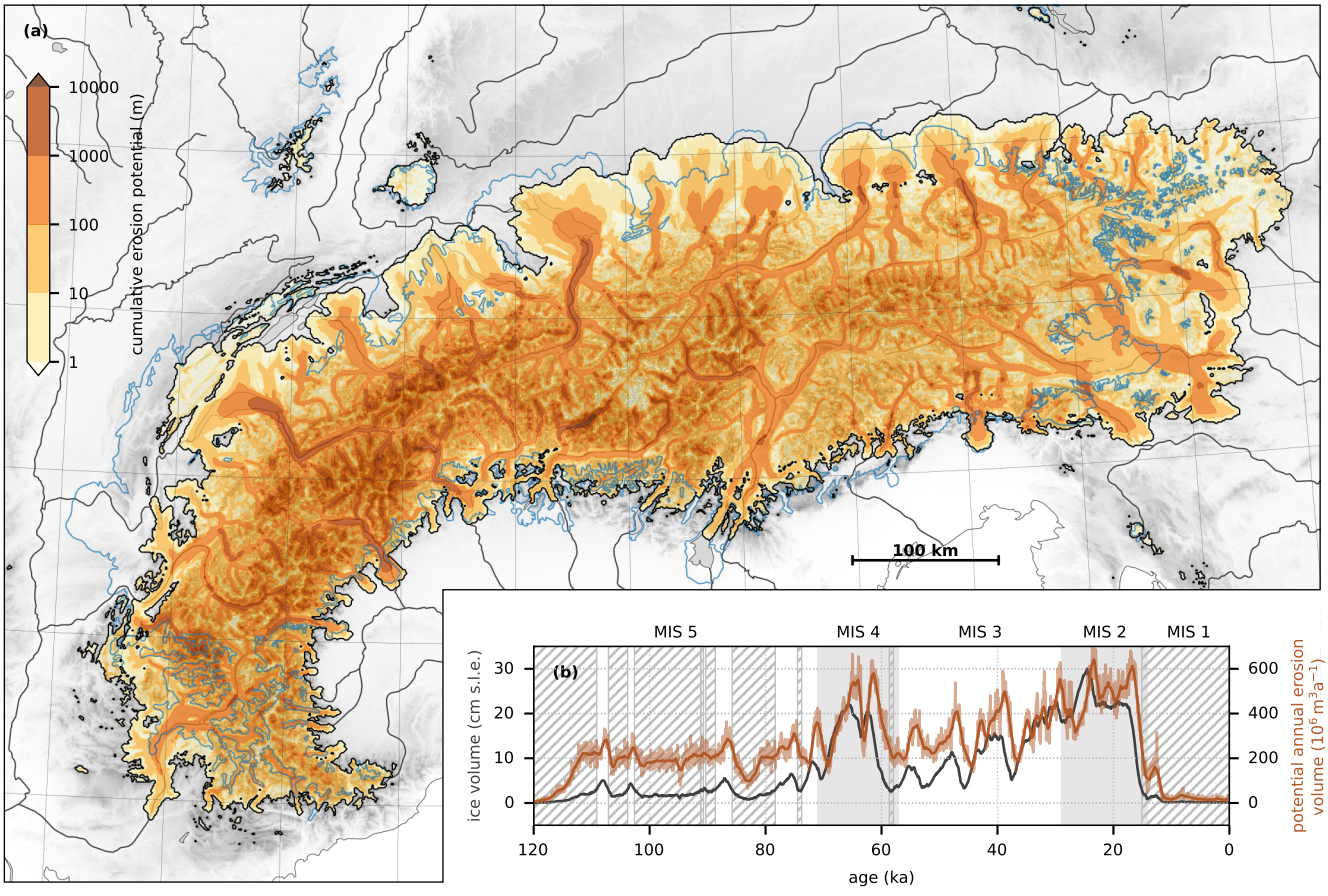

Figure S3. Cumulative erosion potential and annual erosion volume after Humphrey and Raymond (1994)

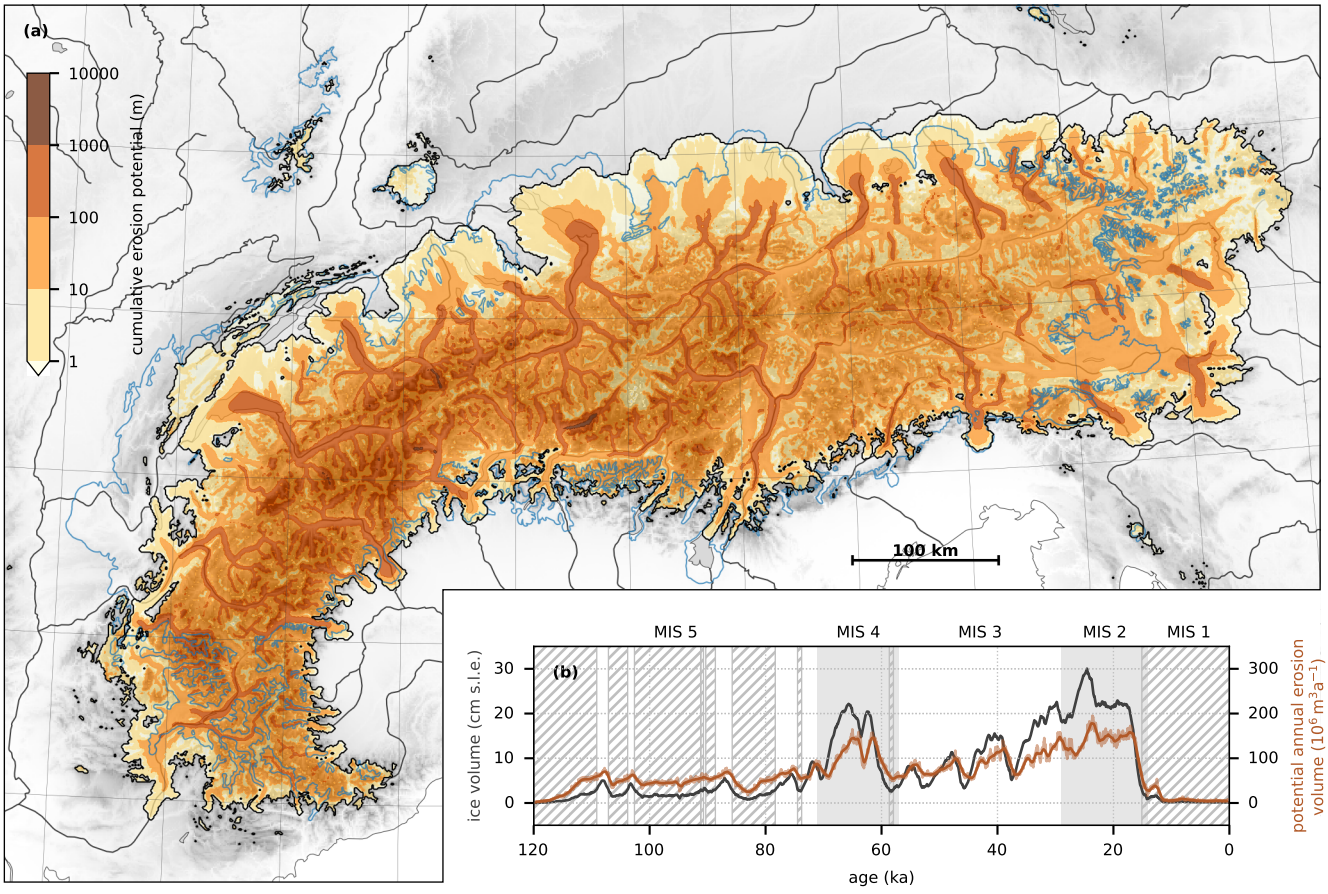

Figure S4. Cumulative erosion potential and annual erosion volume after Cook et al. (2020)

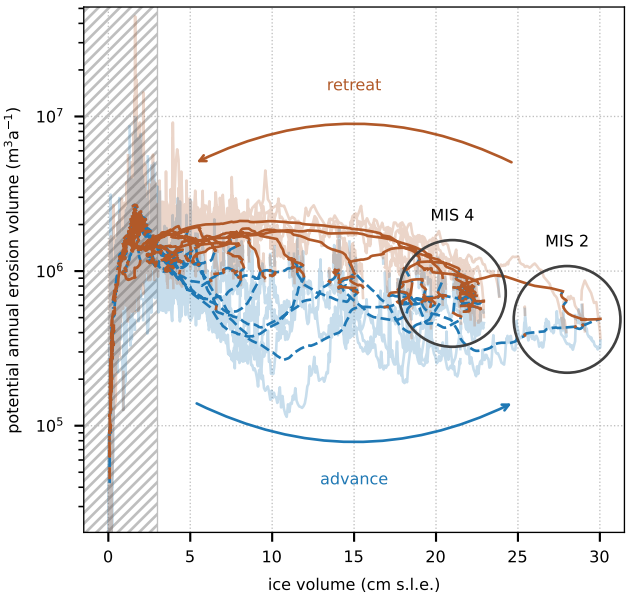

Figure S5. Modelled annual (domain-integrated) potential erosion volume (light curves) and its 1-ka running mean (dark curves) in relation to the modelled total ice volume in centimetres of sea-level equivalent. Blue indicates increasing ice volume and brown decreasing ice volume. After Koppes et al. (2015), same as main text Fig. 2.

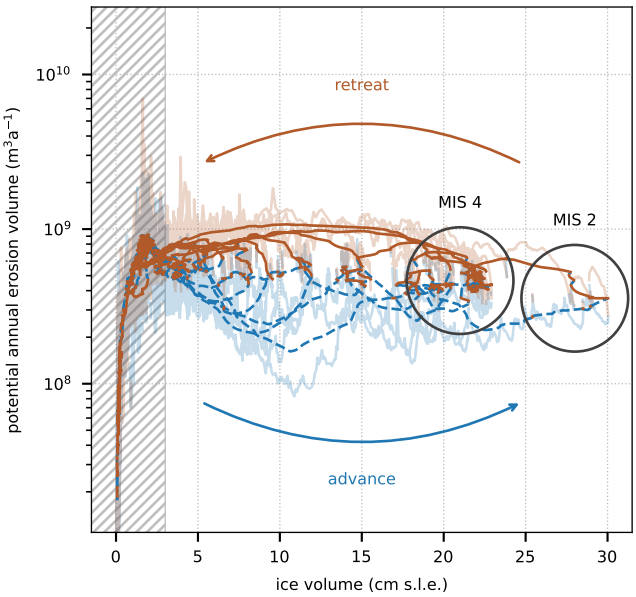

Figure S6. Potential erosion volume in relation to ice volume after Herman et al. (2015).

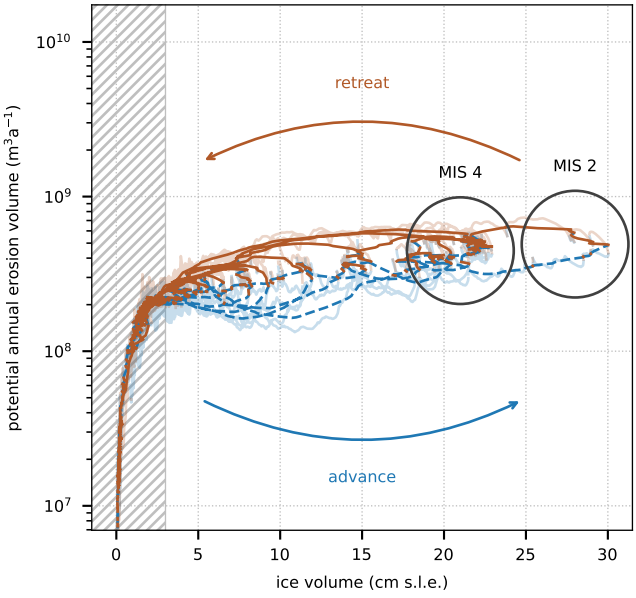

Figure S7. Potential erosion volume in relation to ice volume after Humphrey and Raymond (1994).

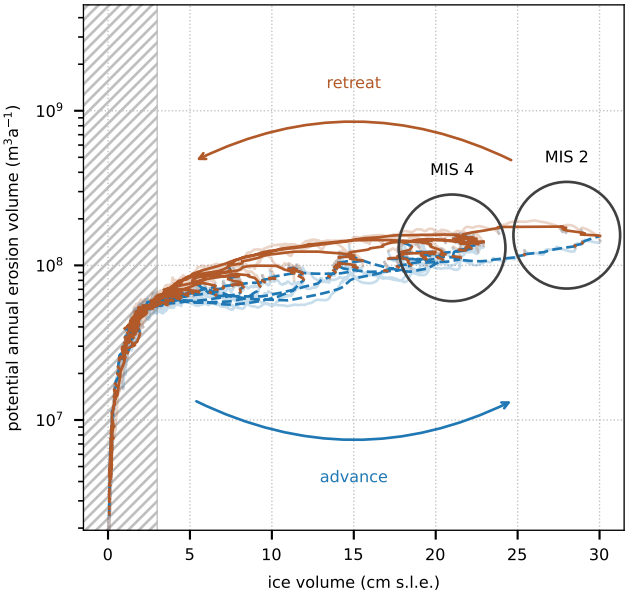

Figure S8. Potential erosion volume in relation to ice volume after Cook et al. (2020).

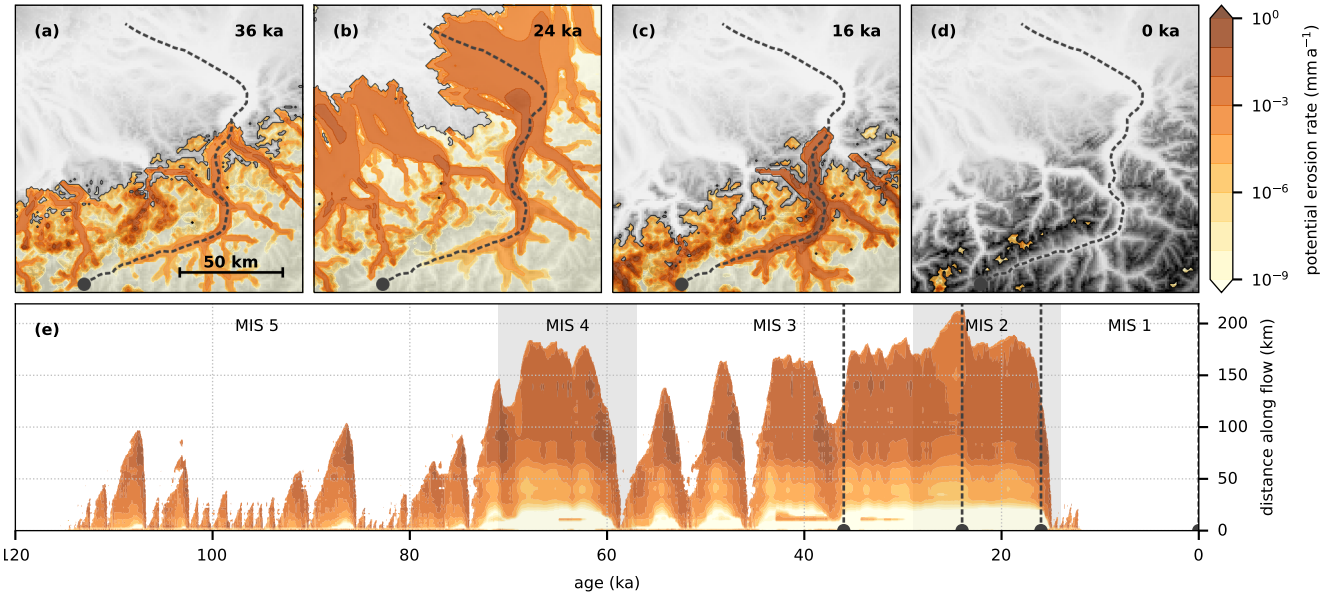

Figure S9. **(a–d)** Modelled instantaneous potential erosion rate of the Rhine Glacier for selected glacier advance and retreat ages, and the final model state for topographic reference. **(e)** Interpolated instantaneous potential erosion rate along a Rhine Glacier transect (upper panels dashed line) for the entire last glacial cycle. After Koppes et al. (2015), same as main text Fig. 3.

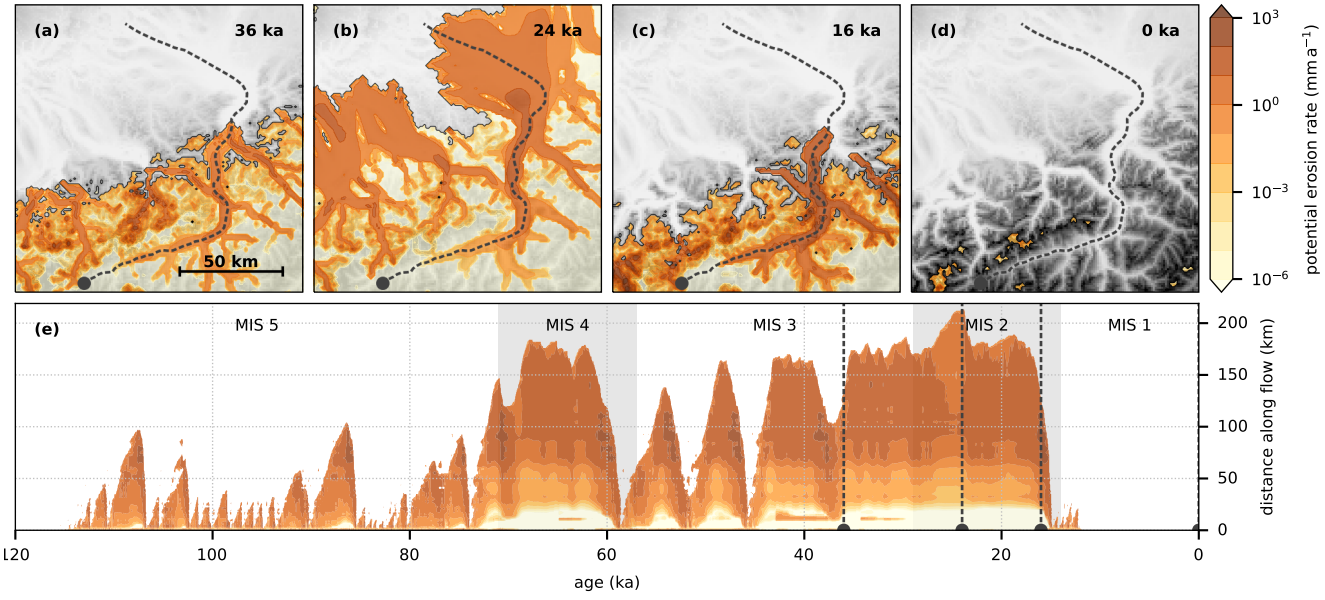

Figure S10. Rhine Glacier potential erosion rate over time after Herman et al. (2015).

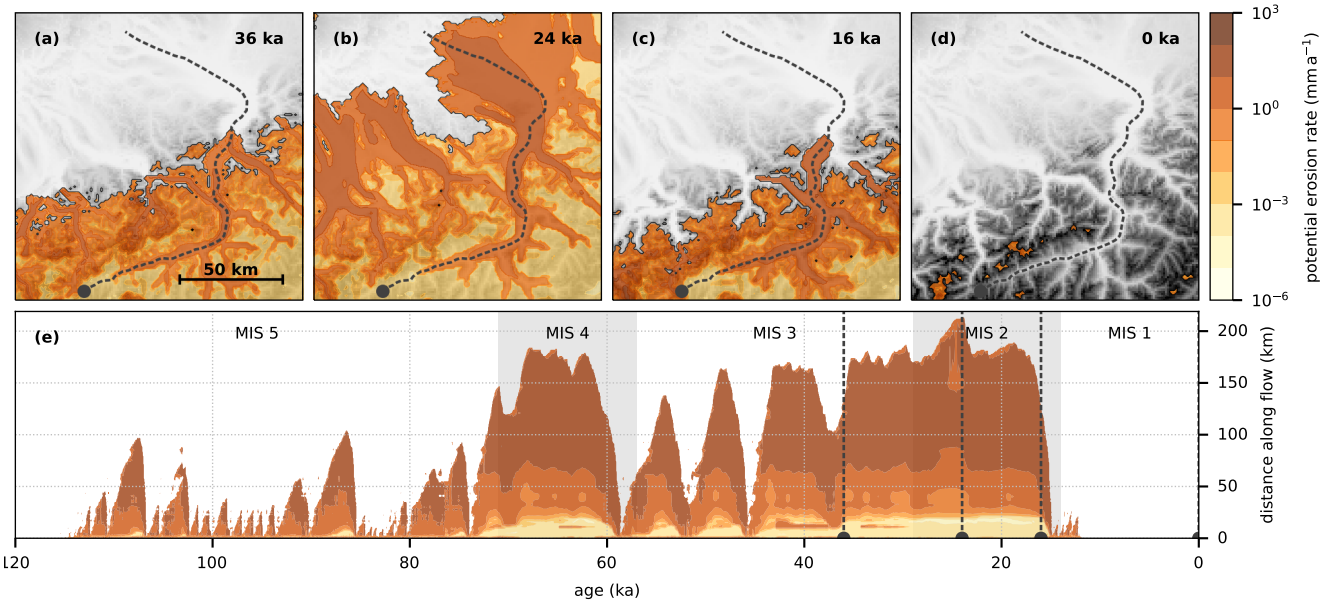

Figure S11. Rhine Glacier potential erosion rate over time after Humphrey and Raymond (1994).

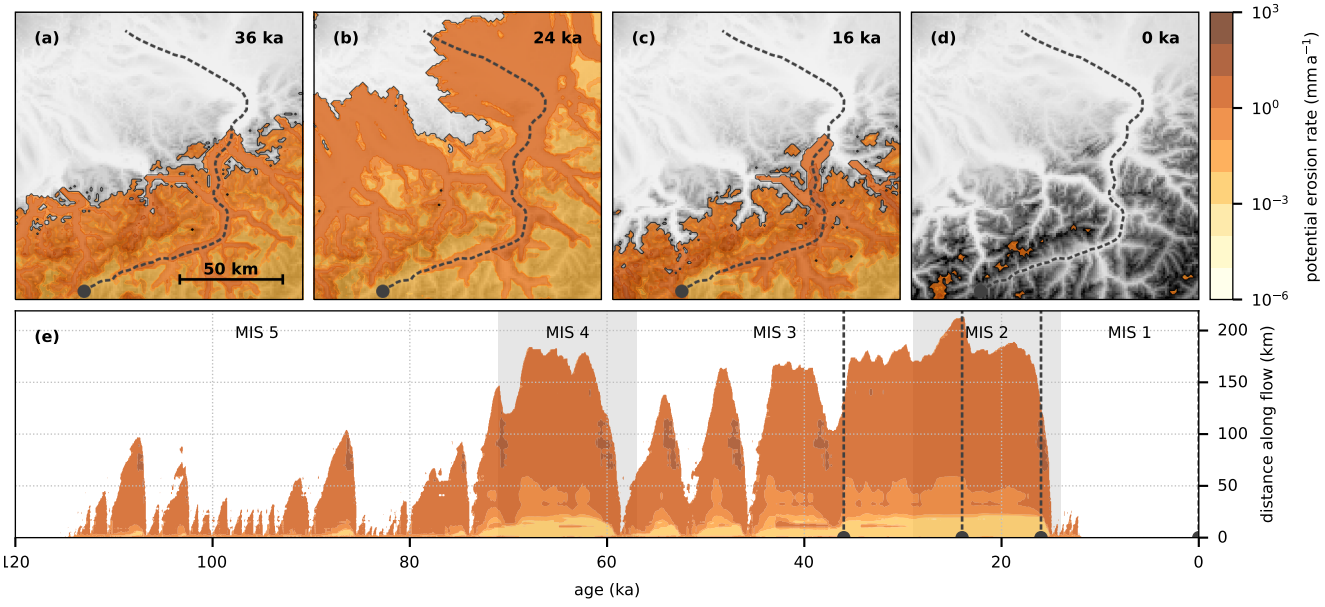

Figure S12. Rhine Glacier potential erosion rate over time after Cook et al. (2020).

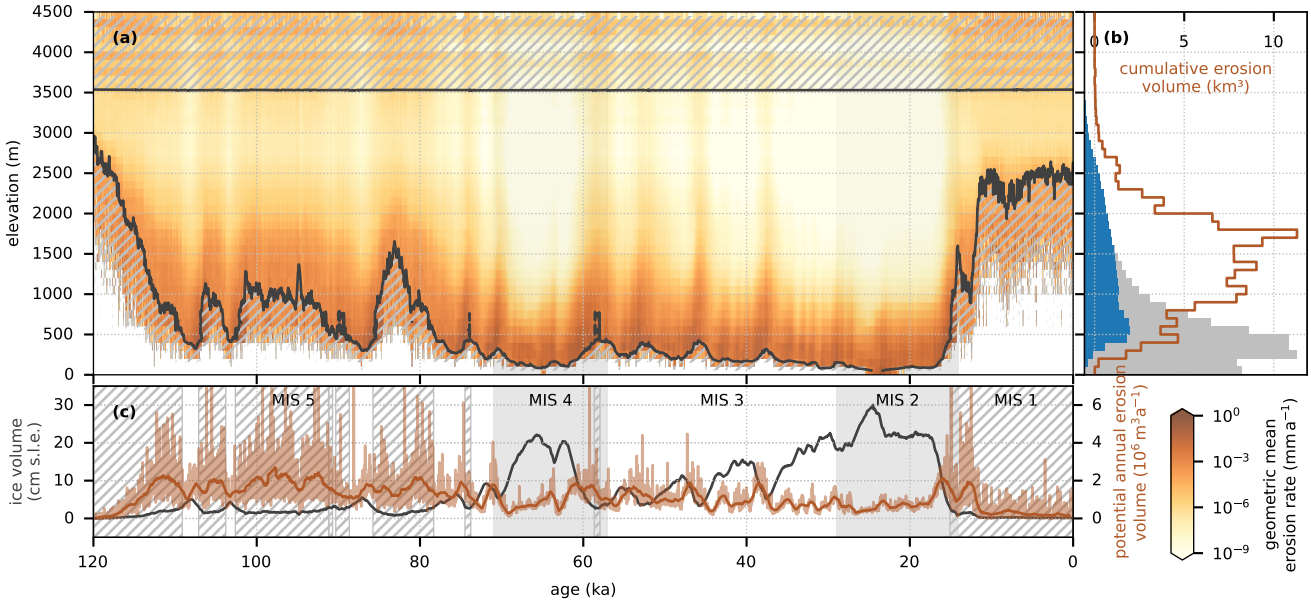

Figure S13. **(a)** Potential erosion rate "hypsogram", showing the geometric mean of modelled rates in 100-m elevation bands across the entire model domain and its time evolution. Hatches indicate elevation bands with fewer than a hundred grid cells (100 km^2). **(b)** Distribution of model domain bedrock topography (grey bars) and glaciated topography (blue bars) in 100-m elevation bands, and the corresponding cumulative potential erosion volume (brown line). **(c)** Same as Fig. S1b. After Koppes et al. (2015), same as main text Fig. 4.

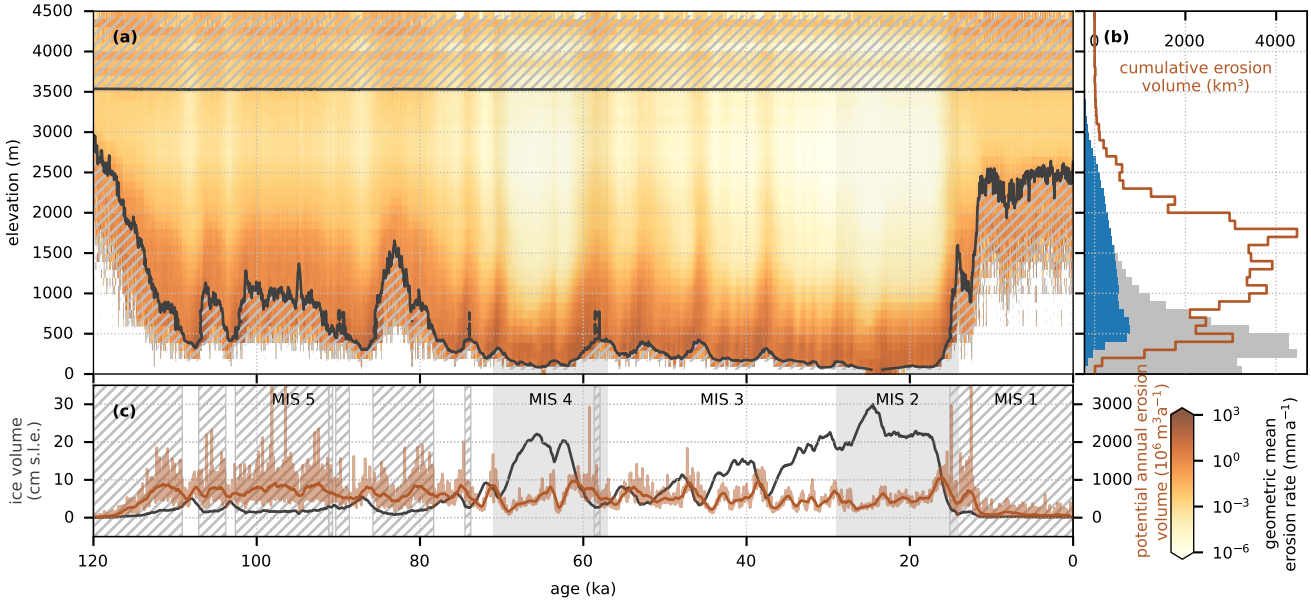

Figure S14. Potential erosion rate per altitude band after Herman et al. (2015).

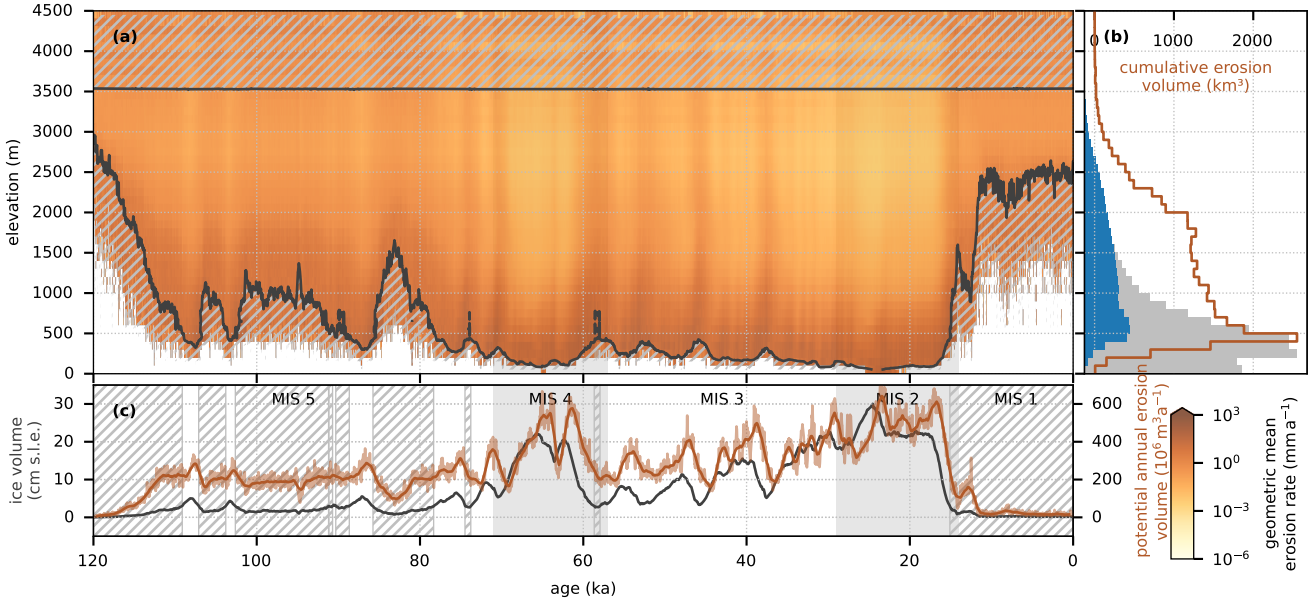

Figure S15. Potential erosion rate per altitude band after Humphrey and Raymond (1994).

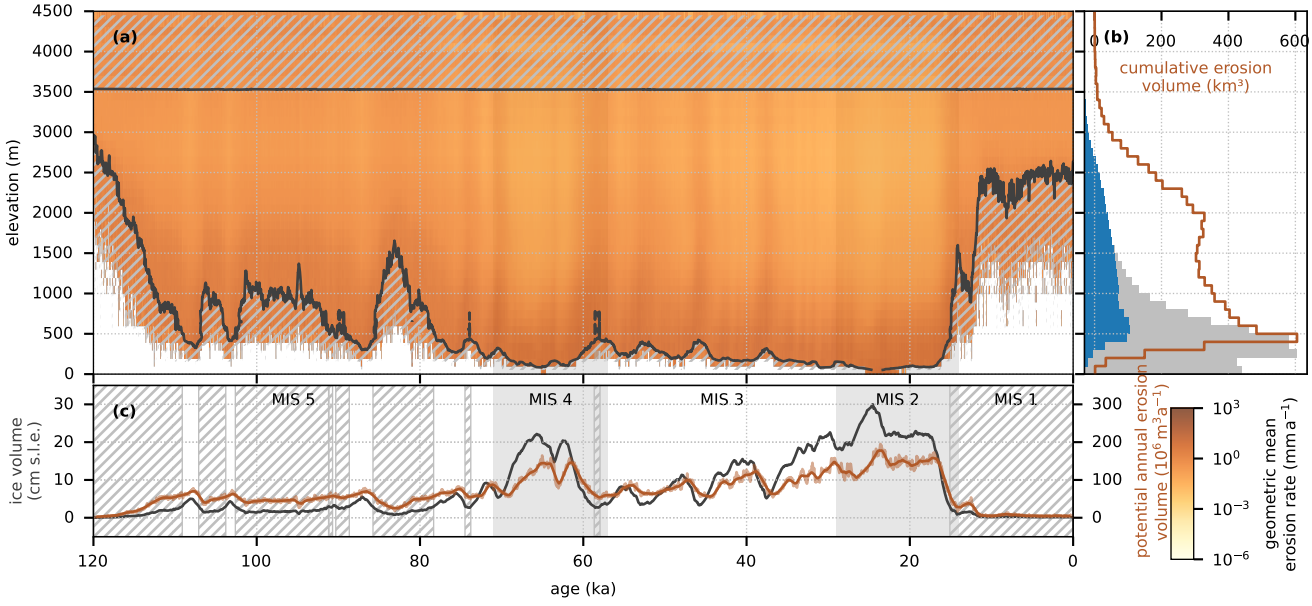

Figure S16. Potential erosion rate per altitude band after Cook et al. (2020).

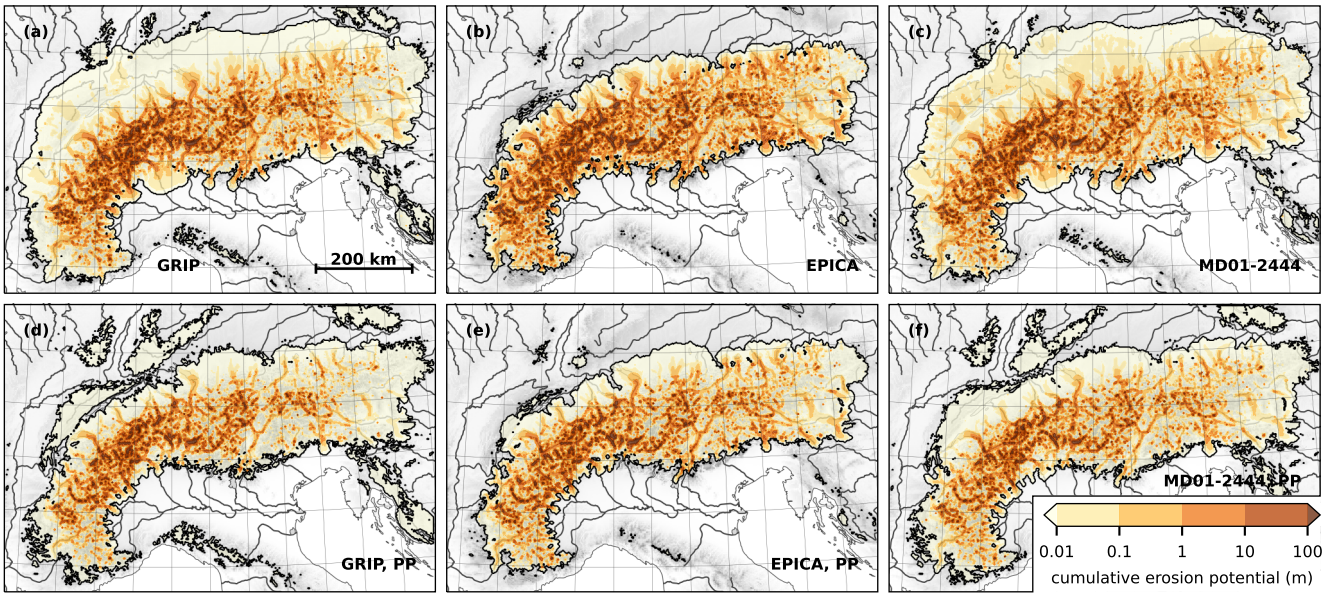

Figure S17. Modelled cumulative glacial erosion potential over the last glacial cycle using three different paleo-temperature histories from **(a, d)** the Greenland Ice Core Project (GRIP; Dansgaard et al., 1993), **(b, e)** the European Project for Ice Coring in Antarctica (our default, EPICA; Jouzel et al., 2007), and **(c, f)** an oceanic sediment core from the Iberian margin (MD01-2444; Martrat et al., 2007), and both **(a–c)** without and **(d–f)** with paleo-precipitation reductions (cf. Seguinot et al., 2018). After Koppes et al. (2015), same as main text Fig. 5.

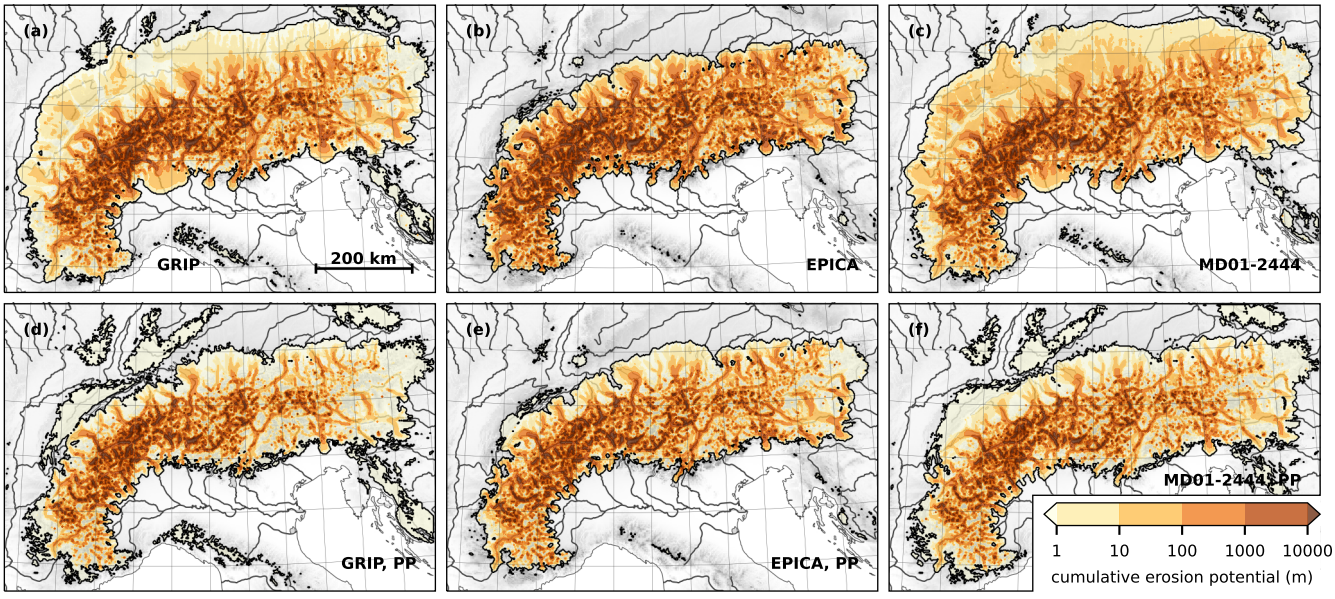

Figure S18. Climate sensitivity of cumulative erosion potential after Herman et al. (2015).

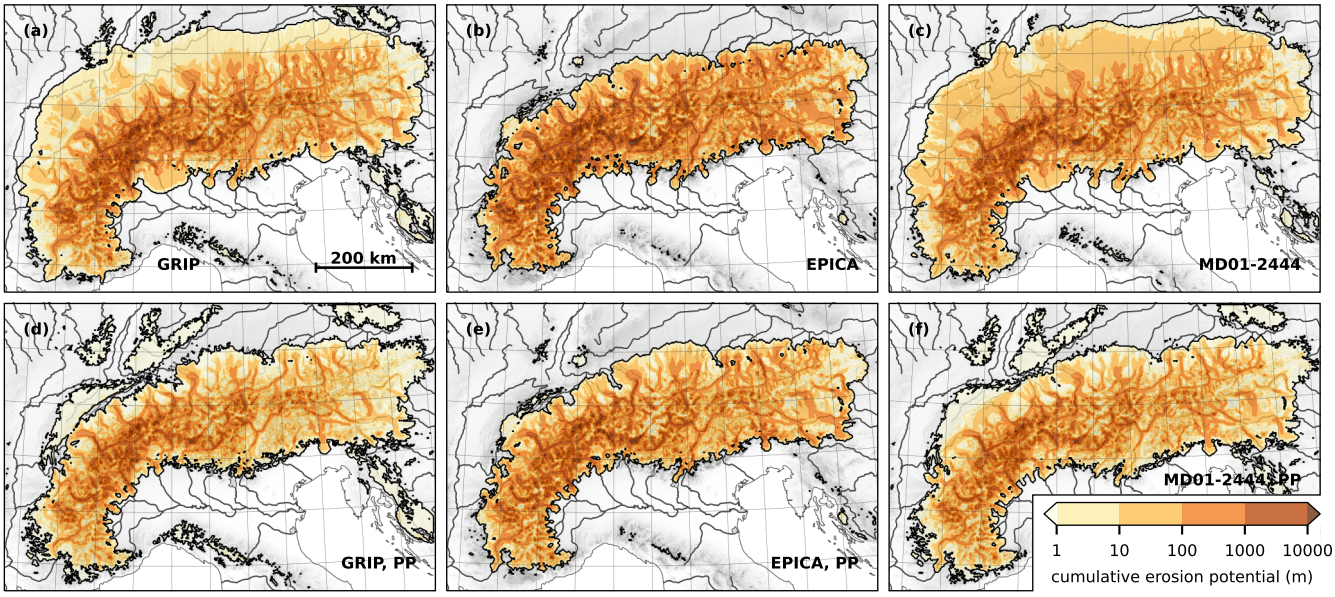

Figure S19. Climate sensitivity of cumulative erosion potential after Humphrey and Raymond (1994)

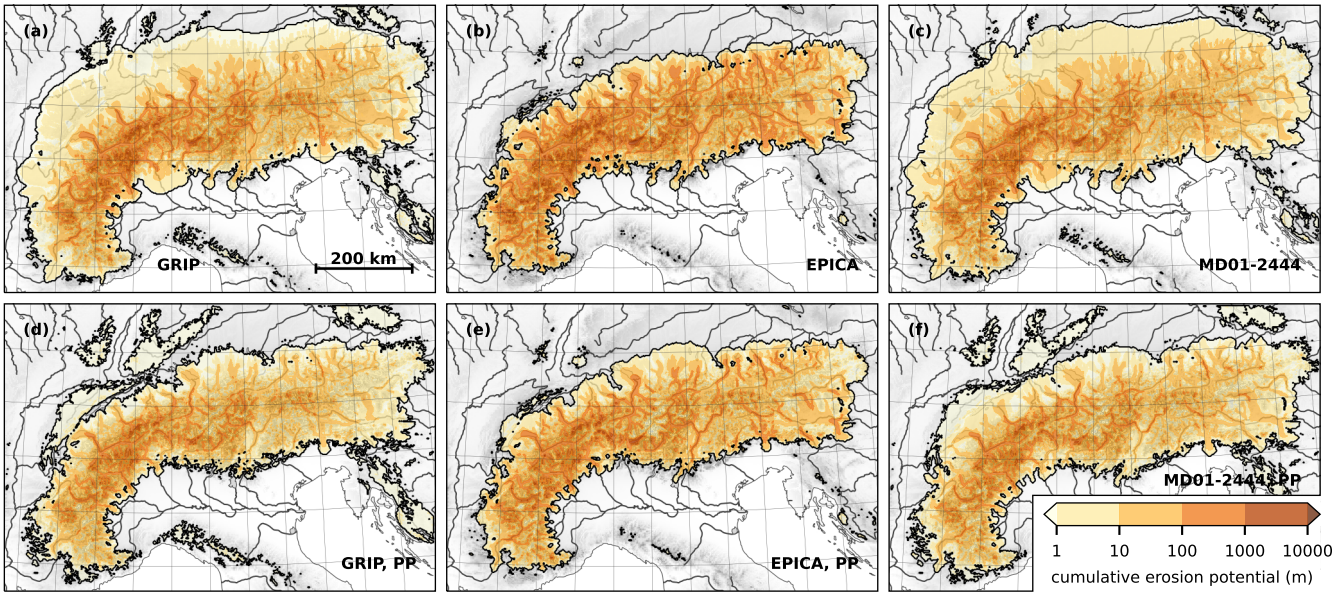

Figure S20. Climate sensitivity of cumulative erosion potential after Cook et al. (2020)

References

Cook, S. J., Swift, D. A., Kirkbride, M. P., Knight, P. G., and Waller, R. I.: The empirical basis for modelling glacial erosion rates, Nature Communications, 11, https://doi.org/10.1038/s41467-020-14583-8, 2020.

Dansgaard, W., Johnsen, S. J., Clausen, H. B., Dahl-Jensen, D., Gundestrup, N. S., Hammer, C. U., Hvidberg, C. S., Steffensen, J. P., Sveinbjörnsdottir, A. E., Jouzel, J., and Bond, G.: Evidence for general instability of past climate from a 250-kyr ice-core record, Nature, 364, 218–220, https://doi.org/10.1038/364218a0, data archived at the World Data Center for Paleoclimatology, Boulder, Colorado, USA., 1993.

Ehlers, J., Gibbard, P. L., and Hughes, P. D., eds.: vol. 15 of *Dev. Quaternary Sci.*, Elsevier, Amsterdam, 2011.

Herman, F., Beyssac, O., Brughelli, M., Lane, S. N., Leprince, S., Adatte, T., Lin, J. Y. Y., Avouac, J.-P., and Cox, S. C.: Erosion by an Alpine glacier, Science, 350, 193–195, https://doi.org/10.1126/science.aab2386, 2015.

Humphrey, N. F. and Raymond, C. F.: Hydrology, erosion and sediment production in a surging glacier: Variegated Glacier, Alaska, 1982–83, J. Glaciol., 40, 539–552, https://doi.org/10.3189/s0022143000012429, 1994.

Jarvis, A., Reuter, H., Nelson, A., and Guevara, E.: Hole-filled SRTM for the globe Version 4, available from the CGIAR-CSI SRTM 90m Database, http://srtm.csi.cgiar.org, 2008.

Jouzel, J., Masson-Delmotte, V., Cattani, O., Dreyfus, G., Falourd, S., Hoffmann, G., Minster, B., Nouet, J., Barnola, J. M., Chappellaz, J., Fischer, H., Gallet, J. C., Johnsen, S., Leuenberger, M., Loulergue, L., Luethi, D., Oerter, H., Parrenin, F., Raisbeck, G., Raynaud, D., Schilt, A., Schwander, J., Selmo, E., Souchez, R., Spahni, R., Stauffer, B., Steffensen, J. P., Stenni, B., Stocker, T. F., Tison, J. L., Werner, M., and Wolff, E. W.: Orbital and Millennial Antarctic Climate Variability over the Past 800,000 Years, Science, 317, 793–796, https://doi.org/10.1126/science.1141038, data archived at the World Data Center for Paleoclimatology, Boulder, Colorado, USA., 2007.

Koppes, M., Hallet, B., Rignot, E., Mouginot, J., Wellner, J. S., and Boldt, K.: Observed latitudinal variations in erosion as a function of glacier dynamics, Nature, 526, 100–103, https://doi.org/10.1038/nature15385, 2015.

Lisiecki, L. E. and Raymo, M. E.: A Pliocene-Pleistocene stack of 57 globally distributed benthic δ^{18}O records, Paleoceanography, 20, PA1003, https://doi.org/10.1029/2004pa001071, 2005.

Martrat, B., Grimalt, J. O., Shackleton, N. J., de Abreu, L., Hutterli, M. A., and Stocker, T. F.: Four climate cycles of recurring deep and surface water destabilizations on the Iberian margin, Science, 317, 502–507, https://doi.org/10.1126/science.1139994, 2007.

Patterson, T. and Kelso, N. V.: Natural Earth. Free vector and raster map data, http://naturalearthdata.com, 2017.

Seguinot, J.: Alpine ice sheet erosion potential aggregated variables [data set], Zenodo, https://doi.org/10.5281/zenodo.4495419, 2021.

Seguinot, J., Ivy-Ochs, S., Jouvet, G., Huss, M., Funk, M., and Preusser, F.: Modelling last glacial cycle ice dynamics in the Alps, The Cryosphere, 12, 3265–3285, https://doi.org/10.5194/tc-12-3265-2018, 2018.